Discrete numerical simulation of fracture propagation in disordered materials: mesh dependency

Jan Eliáš[1,a] and Miroslav Vořechovský [1,b]

[1]Institute of Structural Mechanics, Faculty of Civil Engineering, Brno University of Technology, Veveří 95, 602 00 Brno, Czech Republic

[a]elias.j@fce.vutbr.cz, [b]vorechovsky.m@fce.vutbr.cz

Keywords: lattice models; rigid-body-spring networks; mesh dependency

Abstract. The paper deals with computer simulations of fracture process in concrete. The heterogeneous material is represented by the two-dimensional rigid-body-spring network and the fracture process proceeds by a sequence of linear steps (events) in which elements are removed from the stiffness matrix one-by-one. This simple and well known approach provides realistic crack patterns and model responses. Obviously the solution is influenced by the mesh structure. The paper shows that the crack pattern is chaotically dependent on the network and the dependency of model response on the network element size is discussed as well.

Introduction

The lattice representation of material is a natural alternative to classical approaches. The first simulation of fracture using lattice has been published in theoretical physics in 1989 [1]. Since that time, many types of lattices and fracture criteria have been developed. The applicability of such kind of network models is often restricted by a computer performance. In these days, extensive lattice simulations in 3D are being calculated [2-4].

The most attractive feature of the lattice approach is that the material structure is directly embedded. Consideration of the structure enables application of primitive constitutive laws of all material phases. Indeed, these ideally brittle elements together reflecting the inner structure can exhibit softening at the structural level. However, the correct behavior of simulated specimen/structure is conditioned by an enough detailed representation of the material structure layout. This leads to extreme computational demands because the average lattice element length should not be greater than the minimal aggregate diameter [5].

An advantage of the lattice representation is the ability to predict realistic crack patterns. Many properties of the fracture process zone can also be investigated (see [6]) because the material characteristic length is incorporated by the applied material structure.

The paper focuses on the dependency of obtained solutions on the network without the ambition to present extensive simulations needed for representation of real specimens. The paper starts with a brief description of the model adopted: 2D rigid-body-spring network introduced by Bolander [7]. The influence of network element size on a simulated response is discussed both for a homogenous and disordered material structure. Then, the text deals with a crack pattern dependency on the network structure. Since the material structure is embedded one might expect a unique crack path independent of the selected mesh. We show that the crack pattern (and also the sequence of broken elements) strongly depends on the mesh.

Modeling framework

One can find many types of lattice elements in the literature. The simplest and intuitive element type is a truss element (e.g. [8]). In order to obtain a correct crack pattern it is necessary to use elements that can carry bending moments [9]. There are two main ways how to transmit the bending forces between nodes: one can use (i) beams instead of springs ([10], for instance) or (ii) apply the concept of rigid bodies in which the domain is discretized into interconnected rigid cells that share contact areas. The physical background of the second approach, originally proposed in [11], seems clearer and we use it in this work.

To reduce spurious dependency of the failure pattern on mesh structure, an irregular geometry has been chosen [12]. The only argument to discretize the domain regularly is to avoid difficulties during elastic homogenization [13] but there exists an elegant and strong method to ensure elastic uniformity of the network resting on Voronoi tessellation [6].

The irregular network can be generated simply according to [14]. Here we utilize another algorithm developed in [15] which is able to mesh also nonconvex domains. Nodes are placed into the domain pseudo-randomly with a restriction of minimal mutual distances. This procedure provides a control over the mesh density inside the domain. Then, the connectivity is introduced by local Delaunay triangulation for each node separately. The borders of the domain are included via a set of auxiliary points (see Fig. 1).

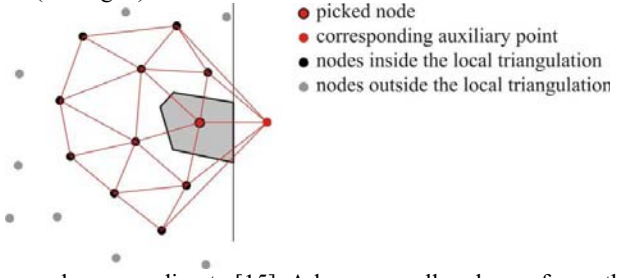

Fig. 1. Tessellation procedure according to [15]. A loop over all nodes performs the local Delaunay triangulation (involving auxiliary points) and subsequently constructs one Voronoi cell in each step.

Since we simulate specimens of laboratory scale, the material meso structure has to be reflected. The material at hand is concrete and so the grain layout has to be represented. Aggregates are computer-generated according to Fuller distribution and placed into the specimen volume by random sequential addition [16], see Fig. 2. The simulated network is then overlaid by the aggregates and the lattice elements are divided into three classes (phases) depending on their position (aggregate, matrix or both).

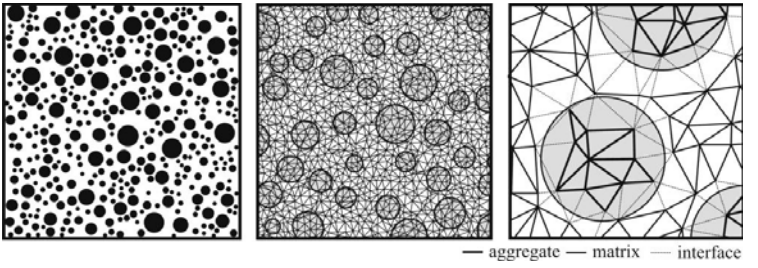

Fig. 2. Left: an example of the computer generated aggregate structure; middle: the network overlaid by the structure of aggregates; right: the separation of the three phases of material.

Fig. 3 shows two connected Voronoi cells. The interactions between cells are ensured by shear and normal springs attached in the middle of the contact lines. Rotational springs are often implemented as well (see [7], for instance) however, in the present model the bending moment is transmitted only using the mentioned translational springs and their eccentricity. All springs are ideally elastic-brittle. The parameters of the springs are set up according to the material phases. The interface elements are the weakest ones. The ratio of spring parameters is adopted from [17]; the particular values are multiplied by a constant to match some experimental responses. The ratio 4:1 used between tensile strengths of the matrix and interface is supported by acoustic emission results [6]. An important part of the model is the failure criterion surface plotted in Fig. 3.

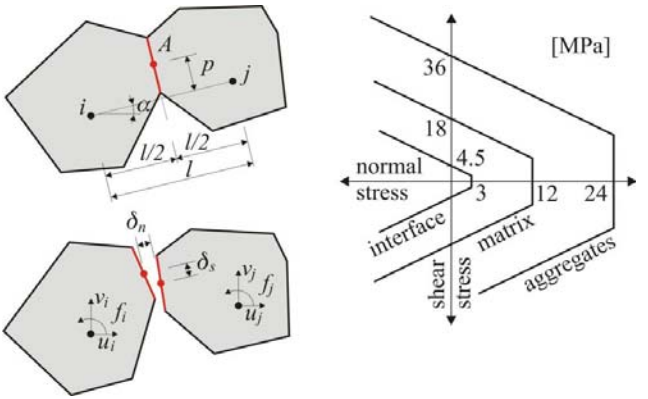

Fig. 3. Left: motion of rigid bodies. Right: element failure criterion surface for the three distinguished material phases.

The solution of response to a proportional loading proceeds in linear steps. First, the network is subjected to a reference load and the connection $c_{i,j}$ with maximal load is found. The step solution is scaled such that the connection $c_{i,j}$ reaches the failure criterion surface. Then the springs of connection $c_{i,j}$ are removed from the stiffness matrix and the next step follows. An example of a solution, obtained for mixed-mode simulation of Nooru-Mohamed test (load-path 6a [18]) is plotted in Fig. 4. The red line represents a smooth response where only steps with an increasing prescribed deformation remain. The same smoothing has been applied to responses from here on.

The lattice works with normal and shear stresses of springs. Article [4] proposed a way to obtain fields of stresses σ_x, σ_y and τ_{xy}. One has to cut the Voronoi cells along two perpendicular lines and find the equilibrium (Fig. 5). In case of a poor discretization the stresses τ_{xy} and τ_{yx} can differ significantly.

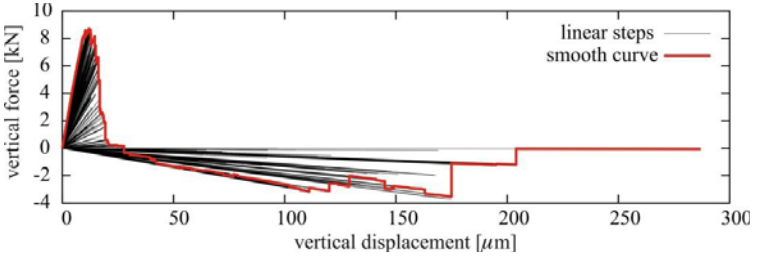

Fig. 4. Plot of linear steps of a mixed-mode simulation. The red line is the smooth solution where only an increasing displacement was accepted.

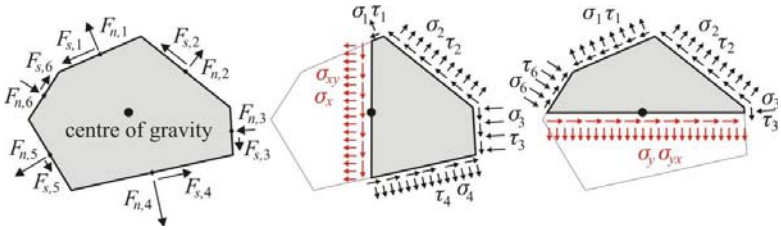

Fig. 5. Nodal stress evaluation. Left: Voronoi cell and corresponding spring forces. Middle and right: components of stress calculated on perpendicular cut faces.

Dependency on element size

The consistent results should be independent of a selected discretization. Surprisingly there are not many articles considering the influence of the network shape and fineness on the lattice simulation results. In order to avoid the dependency on lattice element size the constitutive law can be extended to adopt softening and adopting e.g. the crack band concept [19]. Such an approach is described in [20]. Unfortunately the simplicity of the step-by-step linear solution would be lost then and the softening caused by the material structure would get mixed with the softening from the constituents.

A simple test will now show the strong dependency of our brittle element lattice on the element size. The uniaxial tensile test simulations have been calculated for different discretizations of the domain. The specimen considered is a cube 50×50×50 mm with notches included by removing certain connections along the notch. The mesh size of 1 mm means that the distance restriction applied during node placing algorithm was 1 mm. We have calculated the task for mesh sizes 1.00, 0.50, 0.33, 0.25 and 0.20 mm. The material was considered homogenous in that the aggregate structure was not applied. The obtained responses and crack patterns are plotted in Fig. 7. There is a significant discrepancy between the curves.

The results are not surprising. Fig. 6 is included to elucidate the source of this dependency by showing the fields of principal stress σ_1 on a detail of virtual specimen with a stress concentrator. The same load level causes different stress peaks for various mesh sizes. Since we apply critical stress criteria only, the finer the mesh, the lower load level is needed to further propagate a crack. This problem can be solved using some more sophisticated energetic failure criteria. A homogeneous mesh size independent lattice is published in [21]. It is based on different failure criterion for elements at the crack tip and the rest bulk elements. The springs at the crack tip break when they reach certain energy or, in other words, their tensile strengths are changed based on their length and the characteristic length.

The same task has been calculated also for a heterogeneous lattice. Fig. 7 presents the results for four different mesh sizes. In this case, all the responses judged by diagrams are similar. Also the energies released during the simulations are similar.

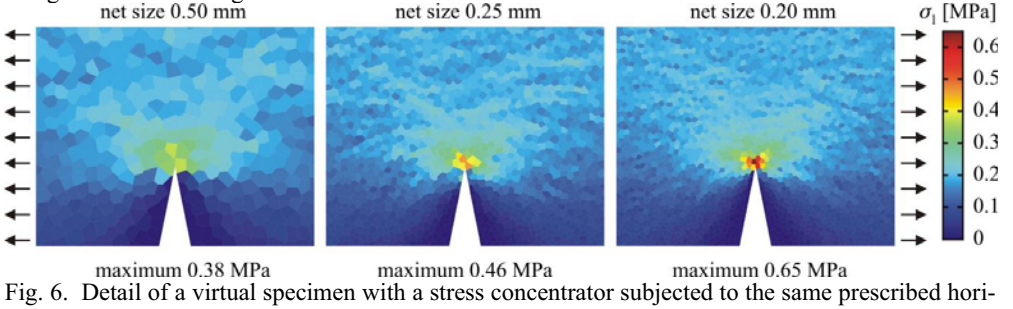

Fig. 6. Detail of a virtual specimen with a stress concentrator subjected to the same prescribed horizontal displacements of supports. The color of Voronoi cells represents the first principal stress.

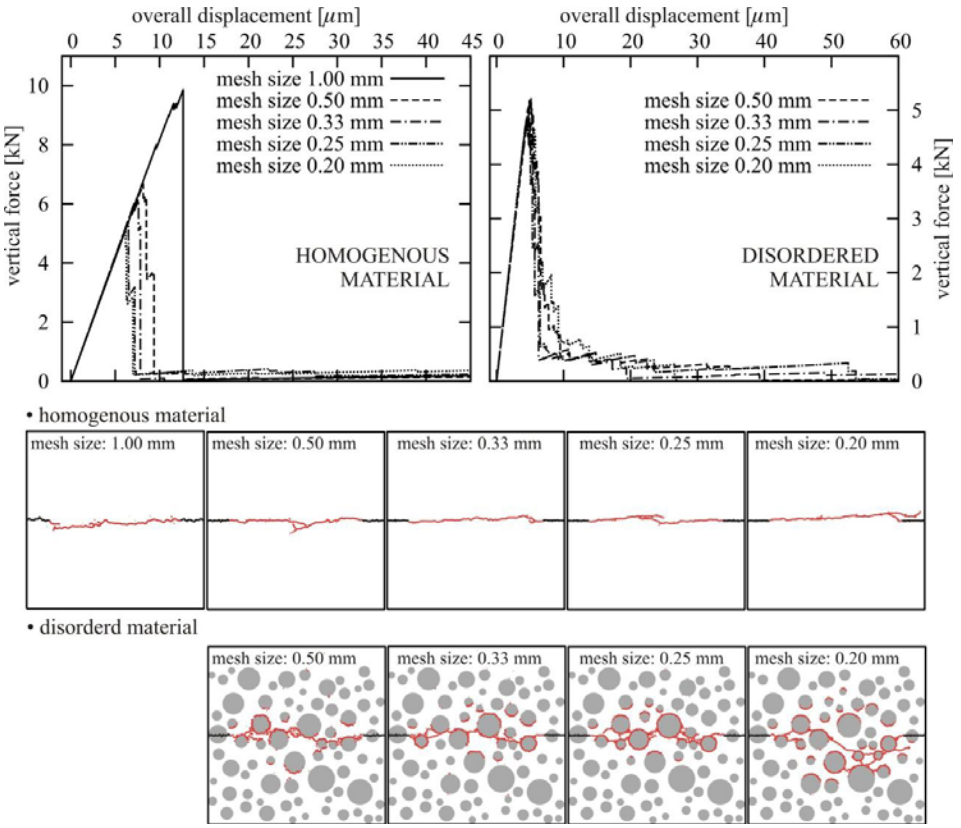

Fig. 7. Demonstration of network element size dependency. Top: Responses of the uniaxial tensile test of virtual notched specimens 50×50×50 mm are plotted for homogenous and disordered materials. Bottom: computed crack patterns.

The main argument is that the irregular aggregate structure, besides others features, reduces the mesh size dependency. We now shall find the limitations of this hypothesis.

Crack pattern variability

The simulations presented in Fig. 7 bottom performed with an identical disordered material structure and varying mesh densities show different crack patterns for different networks. This means that the shape of the crack is not determined solely by the aggregate structure and mechanical properties of the lattice. Unfortunately, it is also driven by the network structure. The following section describes this influence using different networks of identical mesh densities.

In order to analyze the dependency four networks were prepared. The size of the specimen and the load was the same as in the previous section, only the notches were considered already during the tessellation. The reference network, denoted as *A0*, was generated in ordinary way. To obtain the other networks, the nodes from network *A0* were shifted pseudo randomly in both directions. The maximum distance in each direction was 0.1 mm (or 0.01 mm and 0.001 mm) for the net *A01* (or *A001* and *A0001* respectively). The model is based on Voronoi tessellation and therefore the cells had to be generated from scratch. Since the disturbances were quite small, only the amount of

342 elements (or 33 and 1 respectively) of total 9129 elements were replaced by different connectivity of meshes *A01* (or *A001* and *A0001* respectively).
The obtained crack patterns are plotted in Fig. 8. There are some common parts but the general patterns differ. Surprisingly, visual comparison identifies the pattern *A0* closer to *A01* then to the pattern *A0001*. A deeper analysis is showed in Fig. 9. Three plots present comparisons of disturbed networks with the reference one. The steps (events) of both simulations are plotted in parallel with a constant increment. Two events on both parallel coordinates are connected by a line when an identical connection was broken in both networks (the same pair of points were disconnected). One can also see the development of tensile force right below the parallel coordinates graph (only smoothed values are plotted as shown also in Fig. 4). Fig. 9 also compares all responses in a single plot.

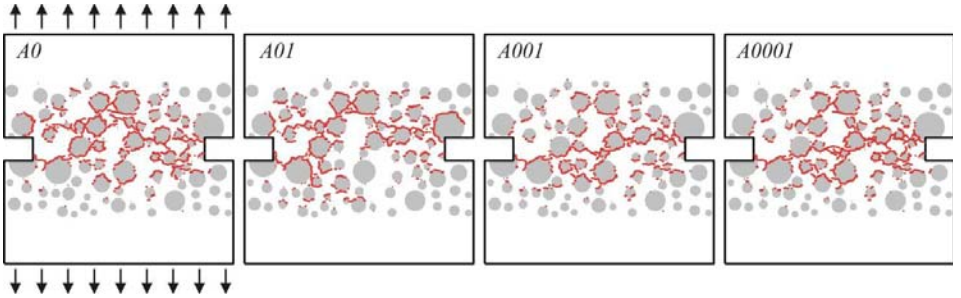

Fig. 8. Crack patterns of simulations with disturbed nodal positions. *A0* is the reference network, nodes in the networks *A01* (or *A001* and *A0001* respectively) are pseudo-randomly shifted in each direction. The maximal shift distance is 0.1 mm (or 0.01 mm and 0.001 mm respectively).

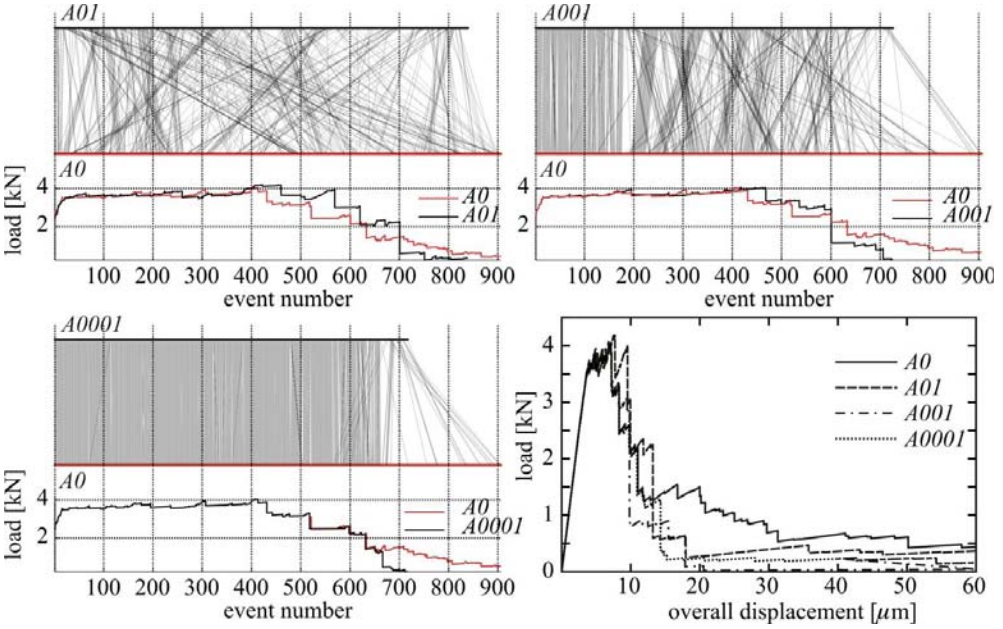

Fig. 9. Comparison of *A* series simulations. The sequence of broken elements in two simulations is compared using parallel coordinates (events with the same broken elements are connected by a line). The development of load is plotted right below the parallel coordinates.

First of all, the discrepancy between the responses is obviously caused only by a few last events. The graphs of load vs. event number for *A0* and *A0001* simulations show a good agreement between the curves except for the last 250 events. Since most of the events are take place around the peak, those 250 events cover 75% of load – displacements graph.

The parallel coordinate plots revealed that the sequence of *A01* events is much further from *A0* than the sequence of *A001* events. This fact again points to the importance of the last few failure events that determine the general crack pattern. The microcracking in simulations *A0* and *A0001* was almost identical, the difference occurs during coalescence into the final macrocrack.

We point finally that the crossing bundles of event connections in the parallel coordinate graph show microcracking at the same location inside the specimen but at different stages of the simulation process.

Summary

The step-by-step linear lattice model has been studied. Reduction of the net element size dependency for disordered materials (using the aggregate structure) has been shown. Limitations of such a reduction deserve further investigation (ongoing work by the authors). The mesh dependency is also exhibited through a variable crack pattern. A nearly chaotic behavior of general crack has appeared: a small disturbance of the network leads to a substantially different macrocrak.

Acknowledgements

The presented work was done during research stay of the first author at the Technical University of Denmark within the Erasmus framework with the financial support of the Ministry of Education of the Czech Republic, project No. 1M06005. Grateful acknowledgements belong to prof. Henrik Stang who supervised this stay. The second author acknowledges financial support received from the Czech Science Foundation under project GACR 103/06/P086.

References

[1] H. J. Herrmann, A. Hansen, S. Roux: Physical review B, Vol. 39 (1989), p. 637-648

[2] G. Cusatis, Z. P. Bažant, L. Cedolin: Journal of Engineering Mechanics, Vol. 129 (2003), p. 1449-1458

[3] G. Lilliu, J. G. M. van Mier: Engineering Fracture Mechanics, Vol. 74 (2007), p. 1174-1189

[4] M. Yip, J. Mohle, J. E. Bolander: Computer-Aided Civil and Infrastructure Engineering, Vol. 20 (2005), p. 393-407

[5] J. G. M. van Mier: *Fracture Processes of Concrete: Assessment of Material Parameters for Fracture Models* (CRC press, Boca Raton, New York, London, Tokyo 1996).

[6] J. E. Bolander, H. Hikosaka, W.-J. He: Engineering Computations, Vol. 8 (1998), p. 1094-1116

[7] J. E. Bolander, S. Saito: Engineering Fracture Mechanics, Vol. 61 (1998), p. 569-591

[8] Z. P. Bažant, M. R. Tabarra, M. T. Kazemi, G. Pijaudier-Cabot: Journal of Engineering Mechanics, Vol. 116 (1990), p. 1686-1705

[9] E. Schlangen, E. J. Garboczi: Engineering Fracture Mechanics, Vol. 57 (1997), p. 319-332

[10] R. Ince, A. Arslan, B. L. Karihaloo: Engineering Fracture Mechanics, Vol. 70 (2003), p. 2307-2320

[11] T. Kawai: Nuclear Engineering and design, Vo. 48 (1978), p. 207-209

[12] M. Jirásek, Z. P. Bažant: Journal of Engineering Mechanics, Vol. 121 (1995), p. 1016-1025

[13] E. Schlangen, E. J. Garboczi: International Journal of Engineering Science, Vol. 34 (1996), p. 1131-1144

[14] C. Mourkazel, H. J. Herrmann: Journal of Statistical Physics, Vol. 68 (1992), p. 911-923

[15] J. E. Bolander, G. S. Hong, K. Yoshitake: Computer-Aided Civil and Infrastructure Engineering, Vol. 15 (2000), p. 120-133

[16] B. Widom: The Journal of Chemical Physics, Vol. 44 (1966), p. 3888-3894

[17] G. Lilliu, J. G. M. van Mier: Engineering Fracture Mechanics, Vol. 70 (2003), p. 927-941

[18] M. B. Nooru-Mohamed: *Mixed-mode fracture of concrete: an experimental approach*, (PhD thesis, Delft University of Technology, Delft 1992)

[19] Z. P. Bažant, B. H. Oh: Materials and Structures, Vol. 16 (1983), p. 155-176

[20] S. Berton, J. E. Bolander: Computer Methods in Applied Mechanics and Engineering, Vol. 195 (2006), p. 7172-7181

[21] A. Jagota, S. J. Bennison: Modelling and Simulation in Materials Science and Engineering, Vol. 3 (1995), p. 485-501